JACS
JOURNAL OF THE AMERICAN CHEMICAL SOCIETY
ARTICLE
pubs.acs.org/JACS

Time-Resolved Small-Angle X-ray Scattering Studies of Polymer−Silica Nanocomposite Particles: Initial Formation and Subsequent Silica Redistribution

Jennifer A. Balmer,[†] Oleksandr O. Mykhaylyk,[*,†] Steven P. Armes,[*,†] J. Patrick A. Fairclough,[†] Anthony J. Ryan,[†] Jeremie Gummel,[‡] Martin W. Murray,[§] Kenneth A. Murray,[§] and Neal S. J. Williams[§]

[†]Dainton Building, Department of Chemistry, University of Sheffield, Brook Hill, Sheffield, S3 7HF, U.K.

[‡]European Synchrotron Radiation Facility, F-38043, Grenoble, France

[§]AkzoNobel, Wexham Road, Slough, Berkshire, SL2 5DS, U.K.

S *Supporting Information*

ABSTRACT:

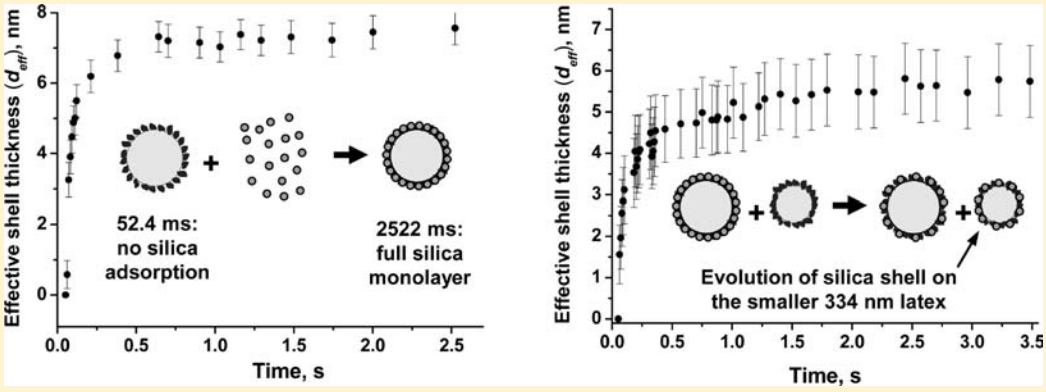

Small angle X-ray scattering (SAXS) is a powerful characterization technique for the analysis of polymer−silica nanocomposite particles due to their relatively narrow particle size distributions and high electron density contrast between the polymer core and the silica shell. Time-resolved SAXS is used to follow the kinetics of both nanocomposite particle formation (via silica nanoparticle adsorption onto sterically stabilized poly(2-vinylpyridine) (P2VP) latex in dilute aqueous solution) and also the spontaneous redistribution of silica that occurs when such P2VP−silica nanocomposite particles are challenged by the addition of sterically stabilized P2VP latex. Silica adsorption is complete within a few seconds at 20 °C and the rate of adsorption strongly dependent on the extent of silica surface coverage. Similar very short time scales for silica redistribution are consistent with facile silica exchange occurring as a result of rapid interparticle collisions due to Brownian motion; this interpretation is consistent with a zeroth-order Smoluchowski-type calculation.

INTRODUCTION

The synthesis, characterization, and structure−property relationships of organic−inorganic colloidal nanocomposites are currently of great interest to both academic and industrial scientists.[1−3] In particular, nanocomposites incorporating ultrafine silica particles have been developed for various potential applications, including photonic devices,[4] synthetic mimics for cosmic dust,[5] and smart Pickering emulsifiers.[6,7] A recent successful commercial application is the use of film-forming nanocomposite particles in high-performance exterior architectural coatings.[8] One of the most well-documented preparation methods involves the in situ aqueous emulsion polymerization of a vinyl monomer in the presence of an ultrafine silica sol to produce core−shell nanocomposite particles. In many early syntheses described in the literature, relatively low silica aggregation efficiencies were obtained,[9−11] meaning that laborious centrifugation−redispersion cycles were required to remove the excess silica prior to characterization of the nanocomposite particles. More importantly, the presence of such excess silica can compromise the performance of nanocomposite particles as Pickering emulsifiers[7] or as tough, transparent

Received: August 3, 2010
Published: December 20, 2010

 © 2010 American Chemical Society

coatings.[12] However, efficient synthesis protocols have now been reported for the preparation of poly(2-vinylpyridine)/silica,[13] polystyrene/silica,[14,15] and poly(styrene-*stat*-*n*-butyl acrylate)/silica[12] nanocomposite particles, whereby silica incorporation efficiencies can exceed 95%.

Recently, we reported an alternative route to core−shell polymer−silica nanocomposite particles that involves the physical adsorption (or heteroflocculation) of ultrafine silica particles onto a preformed sterically stabilized latex in dilute aqueous solution.[16] This approach allows facile variation of the latex core,[17] and optimized protocols can produce a nanocomposite dispersion with little or no excess silica sol.[16] Such nanocomposite particles also exhibit an unprecedented and fascinating phenomenon. Addition of excess sterically stabilized latex to a colloidal dispersion of vinyl polymer−silica nanocomposite particles leads to the spontaneous redistribution of the silica nanoparticles such that *partial* coverage of all the latex particles is achieved.[18] In contrast, silica redistribution does *not* occur upon mixing latex with the equivalent polymer/silica nanocomposite particles prepared via in situ polymerization.[19]

Colloidal dispersions of heteroflocculated poly(2-vinylpyridine)−silica nanocomposite particles have previously been characterized both before and after silica redistribution. The judicious combination of dynamic light scattering (DLS), aqueous electrophoresis, X-ray photoelectron spectroscopy (XPS), and electron microscopy was used to assess the extent of latex surface coverage by the silica particles after nanocomposite formation by heteroflocculation.[16] Silica redistribution between polymer−silica nanocomposites and sterically stabilized latex was investigated using electron microscopy, small-angle X-ray scattering (SAXS), disk centrifuge photosedimentometry (DCP), and XPS.[18,19] However, such "post mortem" analysis of the *equilibrated* colloidal dispersions do not provide any insight into the kinetics of either nanocomposite formation or silica redistribution, other than to confirm that both of these processes appear to be complete within 1 h in dilute solution at 20 °C.

Stopped-flow equipment is commonly used to study the kinetics of processes that occur on short time scales. Rapid mixing of several solutions at different volume ratios can be achieved with short dead times in order to follow the very early stages of a reaction or self-assembly process. The stopped-flow apparatus is easily coupled with a wide range of in-house imaging, spectroscopic, and scattering analysis techniques. For example, Dupin et al. studied the pH-induced swelling kinetics of poly(2-vinylpyridine) latexes by monitoring the turbidimetry changes associated with a pH jump using a commercial stopped-flow instrument.[20] Similarly, Zhang and co-workers used stopped-flow light scattering combined with a fluorescence detector to investigate the pH-responsive micellization kinetics of a pyrene-labeled diblock copolymer.[21] We have shown recently that SAXS is a powerful technique for the analysis of the particle size, polydispersity, and morphology of colloidal nanocomposites.[18] The high electron density contrast between the latex core and the silica shell makes SAXS well-suited for characterizing these nanocomposite particles. Recent advances in detector technology, combined with the high intensity of synchrotron X-ray sources, mean that SAXS can be coupled with stopped-flow apparatus to give millisecond time resolution.[22,23]

Time-resolved SAXS has been widely used to study the growth kinetics of inorganic nanoparticles.[24−26] For example, Pontoni et al. were able to investigate the early stages of in situ Stöber silica growth, as well as observe the overall process, in a single experiment.[24] The earliest analyzable data, obtained within 60 s of mixing equal amounts of alcoholic solutions of ammonia and tetraethyl orthosilicate, corresponded to silica nuclei with a mean radius of around 3 nm. After approximately 120 s, the scattered intensity was found to be well-described by a model for polydisperse spheres of uniform density. The small nuclei subsequently coalesced to form larger particles, as indicated by an increase in radius and a concurrent sharp decrease in the number density of scattering objects. The transformation of mixtures of cationic and anionic micelles to vesicles has also been studied.[27] This involved more complex structural changes than merely the size evolution of spherical particles observed for the Stöber silica growth. By mixing equimolar amounts of cationic and anionic surfactant solutions, relatively monodisperse vesicles were obtained in a multistep reaction. Initially, mixed micelles were formed, the scattering patterns for which were modeled using the form factor for polydisperse hollow shells. These micellar aggregates quickly dissolved to form bilayers that in turn became unilamellar vesicles. It was found that vesicle formation was much slower than the dissolution of the original mixed micelles.

In the current work, time-resolved SAXS is used to follow the kinetics of nanocomposite formation by monitoring the adsorption of 20 nm silica nanoparticles onto 461 nm poly(ethylene glycol) methacrylate-stabilized poly(2-vinylpyridine) [PEGMA-stabilized P2VP] latex particles. The same technique was then applied to the more complex task of studying the spontaneous redistribution of silica that occurs when P2VP−silica nanocomposite particles are challenged by the addition of PEGMA-stabilized P2VP latex.

■ EXPERIMENTAL SECTION

Materials. 2-Vinylpyridine and divinylbenzene (80% divinyl isomer) were purchased from Aldrich. Each monomer was passed through a basic alumina column to remove inhibitor and stored at −25 °C prior to use. 2,2′-Azobis(isobutyramidine) dihydrochloride (AIBA; Aldrich), Aliquat 336 ($N^+[(CH_2)_7CH_3]_3CH_3Cl^-$; Aldrich), and the aqueous silica sol (Bindzil 2040, supplied as a 40 wt % dispersion at pH 10; Eka Chemicals, Bohus, Sweden) were used as received. Monomethoxy-capped poly(ethylene glycol) methacrylate (PEGMA, supplied as a 50 wt % aqueous solution by Cognis Performance Chemicals, Hythe, UK) had a mean degree of polymerization of 45 and an M_w/M_n of 1.10. Deionized water (obtained from an Elgastat Option 3A water purifier) was used in all experiments.

Latex Syntheses. In a typical P2VP latex synthesis, the PEGMA stabilizer (1.00 g of a 50.0 wt % aqueous PEGMA solution) and the cationic Aliquat 336 surfactant (0.50 g) were dissolved in water (38.45 g) in a 100 mL single-necked round-bottomed flask. A comonomer mixture of 2VP (5.00 g) and DVB cross-linker (0.05 g) was then added. The flask was sealed with a rubber septum and the aqueous solution was degassed at ambient temperature using five evacuation/nitrogen purge cycles. The degassed solution was stirred at 250 rpm using a magnetic stirrer and heated at 60 °C with the aid of an oil bath. After 20 min, the initiator solution (0.050 g AIBA dissolved in 5.0 g of water) was added. The polymerizing solution turned milky-white within 10 min and stirring was continued for 24 h at 60 °C. See Table S1 (Supporting Information) for a summary of all the P2VP latexes synthesized in this work.

The P2VP latex particles were centrifuged at 4000−12 000 rpm for 30−45 min, followed by careful decantation of the supernatant, replacement with fresh deionized water, and redispersion of the

sedimented particles with the aid of mechanical rollers. This protocol was used to remove residual 2VP monomer, excess Aliquat 336 surfactant, and nongrafted PEGMA stabilizer. Purification was continued until the serum surface tension was close to that of pure water (71 ± 1 mN m^{-1}), as measured using a surface tensiometer.

Preparation of P2VP−Silica Nanocomposite Particles by Heteroflocculation. All silica adsorption experiments were conducted at pH 10. Under these conditions, both the latex and the silica exhibit negative ζ-potentials.[16] The appropriate volume of a 1.0 w/v % aqueous latex dispersion was added to a known volume of a 1.0 w/v % aqueous silica sol, such that the number of silica particles per latex was equivalent to monolayer silica coverage (i.e., $\Theta = 1.00$) of the latex surface. More specifically, it was assumed that monolayer silica coverage was attained at a silica packing efficiency of $P = 69\%$.[16] Calculations were based on particle diameters measured by dynamic light scattering. For example, 5.00 mL of the 461 nm P2VP latex dispersion (1.0 w/v %) was added to 1.22 mL of 1.0 w/v % aqueous silica sol. These mixtures were homogenized using a vortex mixer at 2000 rpm for 10 s before being allowed to equilibrate on a roller mixer for a minimum of 1 h at 20 °C.

Dynamic Light Scattering (DLS). Studies were conducted at 25 °C using a Malvern Zetasizer Nano ZS instrument equipped with a 4 mW He−Ne laser operating at 633 nm. Backscattered light was detected at 173° and the mean particle diameter was calculated over 30 runs of 10 s duration from the quadratic fitting of the correlation function using the Stokes−Einstein equation. All measurements were performed in triplicate on highly dilute aqueous dispersions.

Field Emission Scanning Electron Microscopy (FE-SEM). Images were obtained using an FEI Inspect instrument operating at 20 kV. Samples were dried onto carbon disks adhered to an aluminum stub and sputter-coated with a thin layer of gold prior to inspection to prevent sample-charging effects.

Transmission Electron Microscopy (TEM). Samples were prepared by drying a drop of a dilute dispersion onto a carbon-coated copper grid. Analyses were conducted using a Philips CM100 electron microscope operating at 100 kV.

Helium Pycnometry. The solid-state densities of the latex particles were determined using a helium pycnometer (Accu Pyc 1330 instrument, Micrometrics). Samples were freeze-dried under vacuum prior to measurement.

SAXS Data Acquisition. SAXS patterns were collected at the European Synchrotron Radiation Facility, at Station ID02 (X-ray radiation wavelength $\lambda = 0.1$ nm, camera length 8 m, cross-section of the beam at the sample holder = 0.3 mm). The X-ray scattering intensity was recorded using a FReLoN (fast-readout low-noise) Kodak CCD detector within a q range of 0.01−0.6 nm^{-1}. The high sensitivity and count rate capability of this detector make it suitable for millisecond time-resolved stroboscopic experiments (see below). The SAXS data was reduced (i.e., normalized, regrouped into one-dimensional patterns, averaged, and background-subtracted) using a utilities software package written by Dr. M. Sztucki.[28] There are inherent limits in the resolution of station ID02 at low q caused by the instrument slits smearing the first few minima of the form factors of both the latex and the core−shell nanocomposite particles; this is especially noticeable at $q < 0.04$ nm^{-1}. Therefore, the data were desmeared prior to analysis using a method developed by Lake.[29] The desmearing procedure was validated by spherical P2VP latex particles used in this study (Figure S1, Supporting Information). The time frames for SAXS data acquisition were varied between 0.1 and 1.0 s to avoid saturation of the detector. *Static* scattering patterns obtained for the starting materials (i.e., silica sol, P2VP latexes, P2VP−silica nanocomposites) before mixing, the silica redistribution experiments at equilibrium (after 1 h at 20 °C), and the solution background (water) were averaged over 10 frames to improve statistics, whereas the *kinetic* scattering patterns obtained during time-resolved SAXS experiments were necessarily single frames collected every 0.1 s.

Scattering patterns for the starting materials and also for the post mortem silica redistribution experiments after equilibration for a minimum of 1 h at 20 °C were collected using the protocol for *static* SAXS measurements described previously.[18] Time-resolved data were obtained using the stopped-flow apparatus as follows (see Figure S2a of the Supporting Information for a schematic representation of the apparatus). Rapid mixing was accomplished using a commercial Bio-Logic SFM-400 stopped-flow instrument consisting of four motorized syringes and three mixers. The last mixer was coupled to a thin-walled flow-through quartz capillary cell (1.4 mm in diameter with a wall thickness of approximately 10 μm). For the analysis of nanocomposite formation, one syringe was filled with a 1.0 w/v % aqueous dispersion of P2VP latex particles and a second syringe was filled with a 1.0 w/v % dispersion of silica nanoparticles. The volume ratios for mixing were selected to ensure monolayer silica coverage.[16] For example, 200 μL of the 450 nm P2VP latex was mixed with 51 μL of the 20 nm silica sol. For the analysis of silica redistribution, one syringe contained a 1.0 w/v % dispersion of P2VP−silica nanocomposite particles and a second syringe contained a 1.0 w/v % dispersion of P2VP latex particles. In this case, the dispersions were mixed in a 1:1 ratio by volume (e.g., 125 μL of each dispersion was mixed together). In all experiments, the remaining two syringes of the four available were filled with deionized water for cleaning the apparatus between runs. This experimental step was also used to monitor solution scattering background through the entire experiment.

After injection of the dispersions via syringe, the sample was allowed to reside in the last mixing chamber for 30 ms. The transfer time from the mixer to the flow-through cell was 2.4 ms; thus, the apparatus had a total dead time of 32.4 ms. Flow was stopped with millisecond precision using a solenoid-driven stopper and data acquisition was synchronized with the mixing sequence of the stopped-flow apparatus. A stroboscopic data collection strategy was adopted (see Figure S2b, Supporting Information): the first data frame was acquired after an initial delay time of 20 ms and thereafter the detector was activated every 130 ms for up to 50 frames (Figure S2b, run 1, Supporting Information). The detector acquisition time was 10 ms. In addition, to obtain temporal resolution in the 10 ms range by filling the gaps in the stroboscopic sequence (120 ms), each mixing experiment was repeated with the first acquisition delayed to 30 (Figure S2b, run 2, Supporting Information), 40, 50 ms, etc., so as to cover the detector readout time. This protocol produced 13 runs in total for each of the studied colloidal dispersions. These individual runs were combined to obtain a full data set for each mixture of dispersions with the first scattering pattern acquired at 52.4 ms, the second frame at 62.4 ms, the third frame at 72.4 ms, and so on.

SAXS Data Analysis. The Irena SAS macros for Igor Pro[30] were used for the modeling and fitting of the SAXS patterns. The scattered intensity $I(q)$ is measured as a function of the X-ray momentum transfer $q = (4\pi/\lambda)\sin\theta$, where 2θ is the scattering angle. In accordance with the software used, the normalized scattering intensity (after subtraction of a solvent background) for a suspension of particles can be represented as

$$I(q) = \sum_{i=1}^{n} S_i(q) N_i \int_0^\infty |F_i^{\mathrm{pop}}(q,r)|^2 \Psi_i(r)\, \mathrm{d}r \qquad (1)$$

where n is the number of different populations of particles in the suspension, N_i is the number density of scattering particles of ith population, $|F_i^{pop}(q,r)|$ is the form factor that describes the particle morphology of the ith population (including contrast and volume parameters of the particles), $\Psi_i(r)$ is the probability size distribution function of scattering particles corresponding to the ith population, and $S_i(q)$ is the structure factor arising from interparticle interactions. In all the experiments described herein, the particle dispersions are relatively dilute. It can be assumed that there are no interparticle interactions, so $S_i(q) \approx 1$ ($i = 1, ..., n$) and $I(q)$ is governed by the form factor of the particles. Therefore, by fitting SAXS data with suitable form factor

models, structural parameters such as particle size and polydispersity can be obtained. The maximum entropy method available for particle size distribution analysis in the Irena SAS package suggested that a Gaussian distribution was an appropriate description of the polydispersities of both the silica sol and the four PEGMA-stabilized P2VP latexes (Table S1, Supporting Information). Thus, a Gaussian was assumed for size distribution functions $[\Psi_i(r)]$ of all particle populations in the analyzed models. Two structural models were exploited in the data analysis: a homogeneous spherical model for the silica sol and the P2VP latex particles and a core−shell model for silica-coated P2VP nanocomposite particles. An extended discussion of the application of the Irena SAS package to similar particle dispersions has been reported previously.[31]

Structural Model Used for Spherical Silica Sol and Latex Particles (Model 1). This model was used to fit the SAXS patterns corresponding to homogeneous spherical particles, which is appropriate for both the silica particles and the P2VP latexes. It should be noted that the PEGMA corona of the sterically stabilized latex particles has a negligible effect on the scattering pattern. An aqueous dispersion of this latex can be represented by a single population of particles in eq 1 (i.e. $n = 1$) with the following functions and parameters describing the model:

$$F^{\mathrm{pop}}(q,r) = V(r)\Delta\rho f(q,r)$$

where

$$f(q,r) = \frac{3[\sin(qr) - qr\cos(qr)]}{(qr)^3}$$

is the form factor of a spherical particle,[32] $V(r) = 4\pi r^3/3$ is the volume of the particles, and $\Delta\rho$ is the scattering contrast between scattering length density of the latex (ρ_c) or silica (ρ_{silica}) and the solvent (ρ_{sol});

$$\Psi(r) = \frac{1}{(2\pi\sigma_R{}^2)^{1/2}}\exp\left[\frac{-(r-R)^2}{2\sigma_R{}^2}\right]$$

is the Gaussian (normal) particle size distribution, where R is the mean particle radius of latex (R_c) or silica (R_{silica}) and σ_R is the standard deviation of the size polydispersity for the particle radius;

$$N = \frac{\nu}{\int_0^\infty V(r)\,\Psi(r)\,\mathrm{d}r}$$

where ν is the relative volume fraction of the particles in the suspension.

Structural Model Used for the Nanocomposite Core−Shell Particles (Model 2). This model (see Figure 1) was used to fit the SAXS patterns corresponding to P2VP−silica nanocomposite particles with a core−shell morphology. It should be noted that the silica shell in these particles is *particulate*. Thus, the scattering intensity of these nanocomposite particles (eq 1) can be represented via a two-population model ($n = 2$), with the first population ($i = 1$) describing the core−shell structure of the particles and the second population ($i = 2$) describing the particulate nature of the shell. This approach had been previously applied successfully to P2VP−silica nanocomposite particles of a different mean diameter prepared by heteroflocculation[18] and also to another core−shell system.[31] The following functions and parameters were used for the model:

$$F_1{}^{\mathrm{pop}}(q,r) = V_{\mathrm{total}}(r)(\rho_{\mathrm{shell}} - \rho_{\mathrm{sol}})f(q,r+d_{\mathrm{eff}}) + V(r)(\rho_c - \rho_{\mathrm{shell}})f(q,r)$$

where $V_{\mathrm{total}}(r) = 4\pi(r + d_{\mathrm{eff}})^3/3$, d_{eff} is the effective shell thickness (since the shell of the nanocomposite particles is inhomogeneous, this parameter is model-dependent), ρ_c is the scattering length density of the core (P2VP latex), ρ_{sol} is the scattering length density of the solvent (water), and ρ_{shell} is the scattering length density of the shell (this parameter has to be adjusted in the model to account for the fact that the space between each silica nanoparticle in the shell is filled with water);

$$\Psi_1(r) = \frac{1}{(2\pi\sigma_{R_c}{}^2)^{1/2}}\exp\left[\frac{-(r-R_c)^2}{2\sigma_{R_c}{}^2}\right]$$

is the Gaussian (normal) latex core size distribution, where R_c is the mean core radius and σ_{R_c} is the standard deviation for the polydispersity of the latex core radius;

$$N_1 = \frac{\nu_{\mathrm{latex}}}{\int_0^\infty V(r)\,\Psi_1(r)\,\mathrm{d}r}$$

where ν_{latex} is the relative volume fraction of the latex cores in the suspension;

$$F_2{}^{\mathrm{pop}}(q,r) = V(r)(\rho_{\mathrm{silica}} - \rho_{\mathrm{sol}})f(q,r);$$

$$\Psi_2(r) = \frac{1}{(2\pi\sigma_{\mathrm{silica}}{}^2)^{1/2}}\exp\left[\frac{-(r-R_{\mathrm{silica}})^2}{2\sigma_{R_{\mathrm{silica}}}{}^2}\right]$$

is the Gaussian size distribution of the silica particles;

$$N_2 = \frac{\nu_{\mathrm{silica}}}{\int_0^\infty V(r)\,\Psi_2(r)\,\mathrm{d}r}$$

where ν_{silica} is the relative volume fraction of the silica particles in the suspension.

Adsorption of Silica Nanoparticles onto P2VP Latex. A self-consistent step-by-step approach was used to obtain structural parameters for the nanocomposite particles formed upon mixing P2VP latex with the silica sol. First, the Irena SAS package was used to fit SAXS patterns obtained for the silica sol and the P2VP latex prior to mixing. For the second step, two sets of parameters (fixed and fitted) were used in model 2 to fit the SAXS patterns obtained for the core−shell nanocomposite particles. The *fixed* parameters were obtained from the first step in the SAXS analysis and other measurements: it is assumed here that the individual silica and latex components do not change in size after formation of the core−shell nanocomposite particles. Thus, the original mean P2VP latex radius is assigned to the nanocomposite core radius (Figure 1a) and the mean silica radius is assigned to the silica particles in the second population. The scattering length densities of both components of the nanocomposite particles were also fixed. On the basis of the chemical composition of the P2VP latex, $(C_7H_7N)_n$, and the P2VP mass density of 1.17 g cm^{-3} determined by helium pycnometry, the scattering length density of the latex was calculated to be $\rho_c = 10.51 \times 10^{10}$ cm^{-2}. Similarly, on the basis of the chemical composition of silica (SiO_2) and an experimental silica mass density of 2.19 g cm^{-3} determined by helium pycnometry, the silica scattering length density was calculated to be $\rho_{\mathrm{silica}} = 18.44 \times 10^{10}$ cm^{-2}. The scattering length density of solvent was calculated to be $\rho_{\mathrm{sol}} = 9.36 \times 10^{10}$ cm^{-2} (taking the mass density of water to be 1.00 g cm^{-3}). It is emphasized that the particulate nature of the shell in these core−shell particles requires two effective parameters in model 2 (d_{eff} and ρ_{shell}) to describe its structure (Figure 1). These two parameters are positively correlated during the adsorption of silica nanoparticles onto P2VP latex. However, the exact relation between these parameters remains unknown; thus, assessment of their correlation in the least-squares fitting of the SAXS data is nontrivial. To overcome this problem, it was necessary to fix one of the parameters in order to stabilize the model fitting. Assuming that all silica in the sample is located within the shell of the

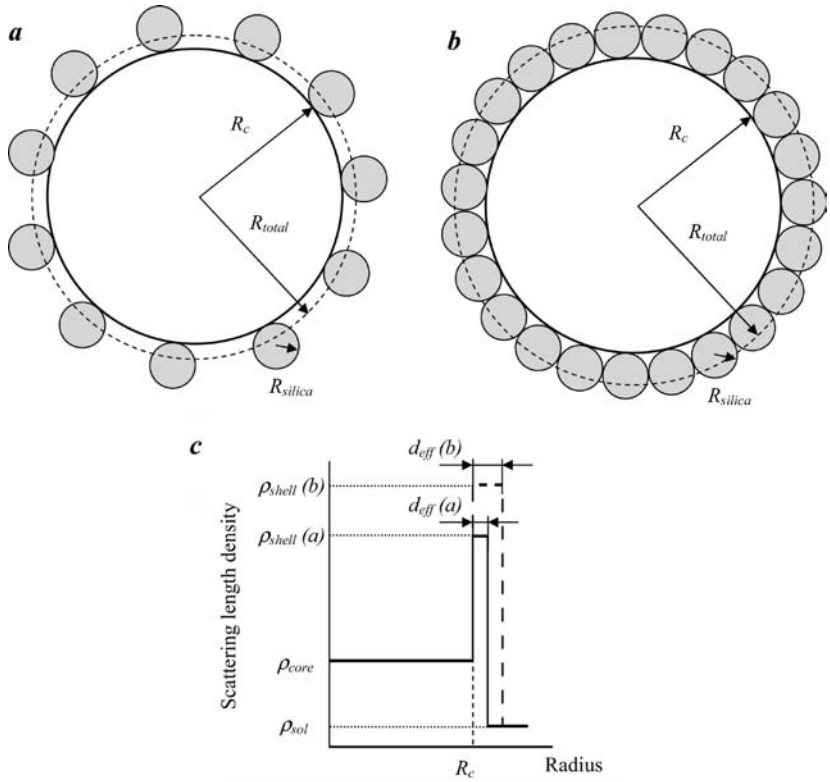

Figure 1. Structural models of the nanocomposite particles used in the SAXS analysis: a core−shell particle with an incomplete (a) and full (b) silica monolayer in the shell and (c) the radial electron density distributions in the corresponding core−shell models of the particles (the related parameters are indicated by the letters a and b).

core−shell nanocomposite particles and that the space between each silica nanoparticle in the shell is filled with water, it was estimated that $\rho_{shell} = 12.73 \times 10^{10}$ cm^{-2}. This is a maximum estimated value for the shell density at full silica monolayer coverage. Although this is not the correct value to fit the scattering patterns obtained during silica adsorption when the latex core is only partially coated with silica, this parameter was fixed in all fittings so as to observe a consistent change in the magnitude of the shell thickness. By fixing ρ_{shell}, the silica shell thickness (d_{eff}) obtained from the fitted model is not an absolute shell thickness but an *effective* shell thickness. In principle, an alternative approach would be to fix the effective shell thickness and allow the electron density to increase with increasing silica coverage during the fitting. However, in practice we found that this led to more ill-defined (i.e., less stable) data fits.

The *fitted* parameters are the following:

d_{eff} is the model-dependent parameter describing the effective thickness of the shell.

v_{silica} is the relative volume fraction of the silica (second population).

v_{latex} is the relative volume fraction of the P2VP latex cores of the nanocomposite particles.

It is not necessary to account for the effect of interparticle correlations between nanocomposite particles as all analyses were conducted on dilute dispersions (1.0 w/v %). However, it might be expected that a Percus−Yevick hard-sphere structure factor[32] would be required to model the interparticle interactions between the close-packed silica particles in the shell in the latter stages of nanocomposite formation. Although the inclusion of a hard-sphere structure factor did produce a good fit to the data for the equilibrium scattering pattern obtained for silica adsorption onto the 461 nm P2VP latex, it was found that the number of silica particles with strong interparticle correlation was low. This is presumably due to the silica polydispersity and their relatively low volume fraction in the suspension. Removing the structure factor from the model did not significantly reduce the quality of the fit. Therefore, the modeling for all scattering patterns in this work was conducted without any hard-sphere structure factor.

Redistribution of Silica Nanoparticles between P2VP Latexes. A similar step-by-step approach was used to analyze the data obtained for the redistribution of silica nanoparticles between P2VP latexes. Size parameters were obtained from fitting the *static* SAXS patterns for the P2VP−silica nanocomposite particles and the P2VP latex prior to mixing. The more complex scattering patterns obtained for these silica redistribution experiments were fitted using a three-population model comprising one population for the larger nanocomposite core−shell particles, a second population for the smaller nanocomposite core−shell particles, and a third population for the particulate silica shell that is present in both partially coated nanocomposites.

Two sets of parameters (fixed and fitted) were used to fit the SAXS patterns obtained for the core−shell nanocomposite particles. The *fixed* parameters were obtained from the first step in the SAXS analysis and other measurements. Again, it was assumed that the latex and silica components do not change in size after forming the core−shell nanocomposite particles. Thus, the mean latex radius is assigned to the core radius of the nanocomposite particles (see Figure 1c) and the mean silica radius is assigned to the silica particles. Scattering length densities of the latex and silica components were fixed as before. The same estimated shell density ($\rho_{shell} = 12.73 \times 10^{10}$ cm^{-2}) was used as a fixed parameter for both nanocomposite populations in the models for all the scattering patterns obtained for the redistribution of silica between latexes, since the intermediate shell densities for all partially coated nanocomposite particles were unknown. Again, this approach ensured that the model fitting was stable, which allowed a consistent

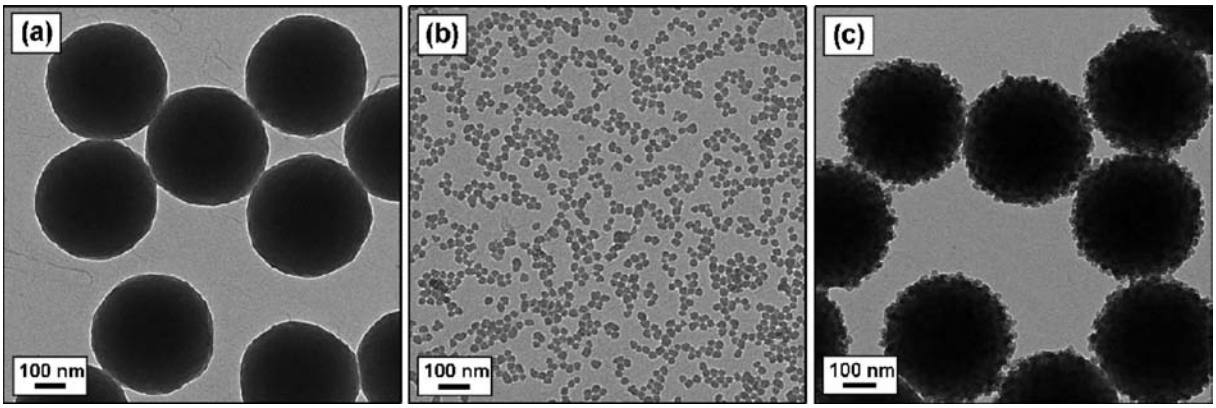

Figure 2. Transmission electron micrographs obtained for (a) a 461 nm PEGMA-stabilized P2VP latex, (b) the 20 nm silica sol, and (c) P2VP−silica nanocomposite particles obtained by the adsorption of 20 nm silica particles onto a 461 nm PEGMA-stabilized P2VP latex (such that the silica surface coverage Θ = 1.00).

increase in the magnitude of the effective shell thickness of the smaller nanocomposite population to be observed.

The *fitted* parameters are the following:

$d_{\mathrm{eff\,616nm}}$ is the model-dependent parameter describing the effective thickness of the silica shell for the larger nanocomposite (the latex core diameter is 616 nm).

$d_{\mathrm{eff\,334nm}}$ is the model-dependent parameter describing the effective thickness of the silica shell for the smaller nanocomposite (the latex core diameter is 334 nm).

v_{silica} is the relative volume fraction of the second population.

$v_{\mathrm{latex\,616nm}}$ is the relative volume fraction of the latex cores of the larger nanocomposite particles.

$v_{\mathrm{latex\,334nm}}$ is the relative volume fraction of the latex cores of the smaller nanocomposite particles.

As discussed for the two-population model used to fit the SAXS patterns obtained for core−shell P2VP−silica nanocomposite particles prepared by heteroflocculation, it was not necessary to add a hard-sphere structure factor to the three-population model used to fit the scattering patterns obtained for the silica redistribution experiments.

■ RESULTS AND DISCUSSION

Kinetics of the Adsorption of Silica Nanoparticles onto P2VP Latex. It has been shown previously that colloidally stable P2VP−silica nanocomposite particles can be successfully prepared by the adsorption of silica onto a PEGMA-stabilized P2VP latex at pH 10.[16] Under these conditions, both the latex and the silica possess negative surface charge; hence, electrostatic interactions are repulsive, rather than attractive. Nevertheless, heteroflocculation is observed because, although latex−latex and silica−silica interactions both give rise to repulsive forces, there is no repulsive force generated during latex−silica interactions (since a steric stabilizer layer can freely penetrate an electrical double layer).

In the present work, the adsorption of 20 nm silica particles onto a 461 nm PEGMA-stabilized P2VP latex was investigated using time-resolved SAXS. TEM images obtained for the latex, silica, and the resulting P2VP−silica nanocomposite particles (where the silica surface coverage, Θ = 1.00) are shown in Figure 2. As expected, the silica nanoparticles are adsorbed onto the latex surface (Figure 2c), with little or no excess silica being present in the dispersion.

SAXS patterns were obtained using the stroboscopic sequence described in the Experimental Section, with the first frame

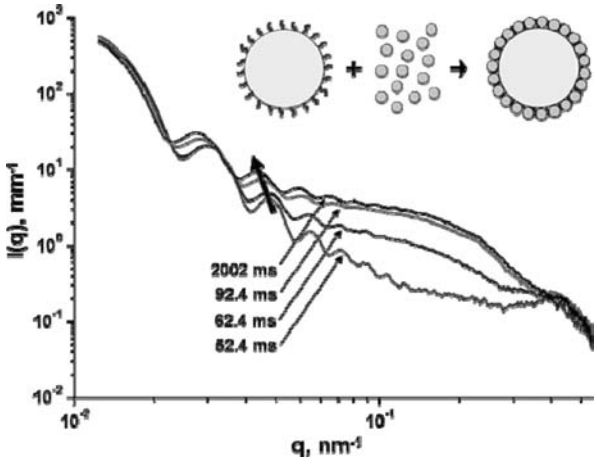

Figure 3. Selected raw SAXS patterns (no background subtraction) obtained during the time-resolved SAXS study of the adsorption of a 20 nm silica sol onto a 461 nm PEGMA-stabilized P2VP latex.

acquired at 52.4 ms. Four of these scattering patterns (raw data; water background not subtracted) are presented in Figure 3 to illustrate the structural evolution of the nanocomposite particles with time. The SAXS pattern obtained at 2002 ms is equivalent to the pattern observed for a 1.0 wt % mixture of the same latex and silica particles that had been allowed to equilibrate for a minimum of 1 h at 20 °C (data not shown). Simply comparing these raw data confirms that time-resolved SAXS is ideally suited for following the kinetics of silica adsorption: a gradual shift in the position of the minima (fringes) of the form factor toward lower q indicates an increase in the overall particle diameter as the silica particles start to coat the latex surface (see the bold arrow in Figure 3).

To ensure that our approach was self-consistent, the particle size parameters obtained from modeling the *static* SAXS patterns obtained for the silica sol and P2VP latex alone (see Table S2, Supporting Information) were used to fit all the scattering patterns obtained during the time-resolved SAXS experiments for the formation of core−shell P2VP−silica nanocomposite particles. With the exception of the very first frame (acquired at 52.4 ms), a good fit to the data was obtained using the same two-population model that had been previously applied to the scattering patterns for P2VP−silica nanocomposite particles at equilibrium (see Figure 4a,b).

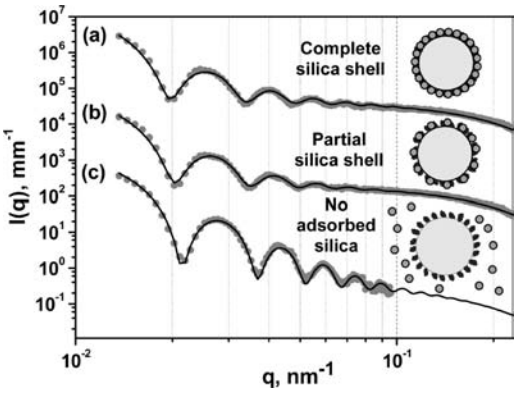

Figure 4. Desmeared SAXS patterns and fits (solid lines) obtained for the adsorption of 20 nm silica particles onto a 461 nm PEGMA-stabilized P2VP latex at (a) 2522 ms, (b) 92.4 ms, and (c) 52.4 ms. Patterns a and b are multiplied by factors of 10 000 and 50, respectively. The noisy part of the scattering pattern of the bare latex (c) has been removed from the plot.

The resulting structural parameters for the frame acquired at 2522 ms are shown in the first row of Table 1. The calculated silica/latex volume ratio is comparable to the predicted ratio, and the silica shell thickness of 7.56 nm is very similar to that obtained for the equivalent P2VP−silica nanocomposite at equilibrium (7.42 nm; see Table S2, Supporting Information). Thus, it appears that a full monolayer of silica has adsorbed onto the P2VP latex approximately 2.5 s after mixing the latex and silica dispersions together. A slightly different two-population model was required to obtain a good fit to the scattering pattern acquired at 52.4 ms (Figure 4c). In this case, a latex population with a spherical form factor (a core−shell form factor with $d_{eff} = 0$) was supplemented by a second population of nonadsorbed silica particles. Thus, it appears that the lower time limit of our experimental setup was just sufficient to briefly observe the binary mixture of latex and silica sol before the silica particles began to adsorb onto the latex surface.

Figure 5 shows a plot of the *effective* silica shell thickness against time. The first scattering pattern, acquired at 52.4 ms, was fitted using a simple spherical form factor for the P2VP latex population, thus the silica shell thickness is zero. For all subsequent scattering patterns, there is a rapid initial increase in effective shell thickness followed by a period of slower growth until an equilibrium is reached at around 500 ms. During the first 250 ms, the shell thickness increases very rapidly, which suggests that the rate of silica adsorption is fast at low silica coverage. At around 250 ms, the rate of growth of shell thickness rapidly decreases until a saturation point is reached at approximately 500 ms. This suggests that, at higher silica coverage, the adsorption of additional silica nanoparticles becomes less favorable. Thus the rate of silica adsorption depends on the extent of silica surface coverage. This is reasonable, because the fraction of bare latex surface that can actually accommodate further silica adsorption will be significantly reduced at higher coverage. Hence, some degree of lateral movement of silica particles over the latex surface may be required to create sufficient space for further silica adsorption to occur.

The deposition of colloidal particles on substrates is often interpreted using a random sequential adsorption (RSA) model.[33] In this approach, hydrodynamic and electrostatic interactions are neglected, and the particles are treated as hard spheres.[34] The particles are sequentially placed at random onto the target and permanently fixed; every position on the target is accessible with equal probability.[34] If a newly adsorbed particle overlaps with any previously adsorbed particles, then it is immediately removed (i.e., it is judged that no adsorption occurs). This process continues until no more particles can be accommodated and the "jamming" packing limit is attained. The RSA maximum packing efficiency for disks placed onto a *planar* surface is $P = 0.55$. Modeling in 3D can only be achieved using computer simulations.[34] However, based on these assumptions, the RSA model appears to be too simplistic for our system. It is probable that the silica nanoparticles are not srtongly adsorbed on the latex surface, as the interaction with the PEGMA chains is relatively weak. The experimental packing efficiency of $P = 0.69$ estimated previously[16] for the adsorption of silica onto P2VP latex suggests that a higher silica surface coverage than that predicted by the RSA model can be attained. This may indicate that the adsorbed silica particles are not pinned to the latex surface: weak adsorption may allow sufficient lateral mobility to enable some relaxation to occur, hence facilitating subsequent silica deposition.

A modified version of the RSA model has also been presented in the literature.[35−37] The ballistic deposition model allows incoming particles to alter their path so as to be less likely to overlap with a previously adsorbed particle. This "restructuring" leads to the slightly higher packing efficiency of $P = 0.61$.[36] This alternative model was applied to the deposition of 406 nm diameter *latex* particles onto *silica* surfaces by Cross et al.[35] A plot of $\ln(\Theta_{max} - \Theta_t)$ against time, where Θ_{max} is the maximum surface coverage and Θ_t is the surface coverage at time t, showed linear dependence, thus suggesting that the ballistic deposition model was applicable to this system. Figure S3 (Supporting Information) shows the equivalent plot for the data obtained from our time-resolved SAXS study of the adsorption of silica onto the 461 nm P2VP latex, where Θ_{max} is the maximum shell thickness and Θ_t is the shell thickness obtained at time t. A linear plot is not obtained, which indicates that the ballistic deposition model is not an adequate description of the silica adsorption process in this case. There is some evidence for linearity at $t <$ 150 ms when silica coverage is low, but thereafter the rate of silica adsorption depends markedly on surface coverage. This is reasonable, as it is likely that electrostatic repulsion between the already adsorbed anionic silica particles and the incoming silica particles increases at higher surface coverage. Thus, we conclude that a more complex model is required to adequately describe silica adsorption onto sterically stabilized P2VP latexes.

The maximum effective silica shell thickness of approximately 8 nm, obtained from the model fitting, is somewhat lower than the shell thickness that might be expected, bearing in mind that the silica particle diameter is 20 nm. This is because the highest possible scattering length density for the shell was used as a fixed parameter in our models. However, this discrepancy in the relative magnitude of the silica shell thickness should not affect our monitoring of the kinetics of silica adsorption. With regard to the reproducibility of our time-resolved SAXS experiments, it is important to note that the data points in Figure 5 are obtained from the summation of nine separate experiments (as discussed in the Experimental Section, the first acquisition for each experiment was recorded at a different time in order to fill the gaps in the stroboscopic sequence). The overall data set has relatively low scatter, indicating that the rapid mixing within the stopped-flow apparatus and subsequent silica adsorption kinetics are indeed reproducible.

Table 1. Summary of the Parameters Used To Model the SAXS Patterns at Selected Times during the Time-Resolved Experiments

	population 1			population 2		population 3			volume ratios			
									silica:latex		latex 2:latex 4	
P2VP−silica sample[a]	core radius R_c (nm)	σ_{R_c} (nm)	shell thickness[b] d_{eff} (nm)	core radius R_c (nm)	σ_{R_c} (nm)	core radius R_c (nm)	σ_{R_c} (nm)	shell thickness[b] d_{eff} (nm)	fitted	predicted	fitted	predicted
prepared with the 461 nm latex at 2.52 s	209.3	5.31	7.56 ± 0.47	11.4	2.79				0.20 ± 0.02	0.129		
prepared with the 216 nm latex at 1.22 s	92.2	4.72	5.73 ± 0.44	11.4	2.79				0.13 ± 0.01	0.152		
prepared with the 616 nm latex and added to the 334 nm latex at 3.48 s	287.9	7.45	4.50 ± 0.88	11.4	2.79	148.3	2.76	5.74 ± 0.84	0.07 ± 0.01	0.048	0.55 ± 0.2	0.54
prepared with the 334 nm latex and added to the 616 nm latex at 3.46 s	148.3	2.76	7.06 ± 1.05	11.4	2.79	287.9	7.45	4.08 ± 1.11	0.14 ± 0.02	0.093	0.49 ± 0.2	0.54

[a] All samples were analyzed as 1.0 w/v % aqueous dispersions. [b] The shell density in all cases was $\rho_{shell} = 12.73 \times 10^{10}$ cm^{-2}.

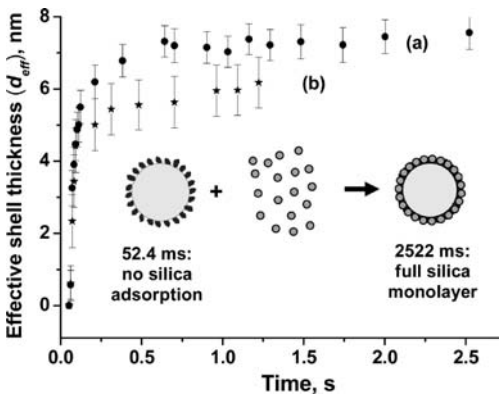

Figure 5. Effective silica shell thickness versus time for the time-resolved SAXS analysis of the adsorption of 20 nm silica particles onto (a) a 461 nm PEGMA-stabilized P2VP latex and (b) a 216 nm PEGMA-stabilized P2VP latex (up to 2522 ms).

The adsorption of 20 nm silica particles onto a 216 nm PEGMA-stabilized P2VP latex was also investigated using time-resolved SAXS. The first frame (acquired at 52.4 ms) was fitted with a two-population model in which a latex population with a spherical form factor was supplemented by a second population of nonadsorbed silica particles. All other scattering patterns were fitted using a two-population model in which a nanocomposite population with a core−shell form factor was supplemented by a second population of adsorbed silica particles. The resulting structural parameters for the frame acquired at 1222 ms are shown in the second row of Table 1. The calculated silica/latex volume ratio is comparable with the predicted ratio, and the silica shell thickness of 5.73 nm is comparable to that obtained for the equivalent P2VP−silica nanocomposite at equilibrium (6.22 nm; see Table S2, Supporting Information). A plot of the *effective* silica shell thickness against time is shown in Figure 5, alongside the equivalent data for the adsorption of silica onto the 461 nm P2VP latex for comparison. It should be noted that the final effective shell thickness for the smaller nanocomposite is less than that of the larger nanocomposite because the specific surface area of the 216 nm P2VP latex is higher, so there is insufficient silica present to form a full monolayer on the 216 nm P2VP latex. When $\Theta = 1.00$ for the nanocomposite prepared using the 461 nm P2VP latex, its silica content is 20 wt %. However, when $\Theta = 1.00$ for the nanocomposite prepared using the 216 nm P2VP latex, its silica content is 36 wt %. Thus, in order to make a more direct comparison between the kinetics of silica adsorption for both latexes, less silica was added to the 216 nm latex so that the silica/latex volume ratio was similar in both systems. The plots shown in Figure 5 suggest that the rate of silica adsorption is independent of latex diameter: in both cases a plateau in the effective shell thickness is observed at around 500−600 ms.

Kinetics of the Redistribution of Silica Nanoparticles between P2VP Latexes. These nanocomposite particles prepared by heteroflocculation are subject to a rather unusual phenomenon: addition of excess PEGMA-stabilized P2VP latex to a colloidal dispersion of P2VP−silica particles leads to spontaneous redistribution of the silica nanoparticles such that *partial* coverage of all the latex particles is achieved. The redistribution of silica between PEGMA-stabilized P2VP latexes has previously been observed by electron microscopy, disk centrifuge, and SAXS.[18,19] However, these post mortem studies of the *equilibrated* colloidal nanocomposite particles have hitherto provided little insight into the kinetics of silica redistribution. In the present work, the redistribution of silica that occurs when a P2VP−silica nanocomposite (prepared by the adsorption of 20 nm silica onto a 616 nm PEGMA-stabilized P2VP latex) is challenged by the addition of a 334 nm PEGMA-stabilized P2VP latex was monitored using time-resolved SAXS. The clear difference in size between the two latexes allows them to be used as "markers", whereby the redistribution of the silica particles before, during, and after mixing can be monitored. Field emission scanning electron microscopy (FE-SEM) images of the original nanocomposite particles, the bare sterically stabilized latex, and the final colloidal nanocomposite particles obtained after mixing these two components are shown in Figure 6.

Earlier static SAXS experiments confirmed unambiguously that silica exchange occurs at 20 °C within 1 h. For the time-resolved studies, rapid efficient mixing of the nanocomposite dispersion with the bare sterically stabilized latex particles was achieved using the stopped-flow apparatus and the first SAXS pattern was acquired at 52.4 ms. Three SAXS patterns (raw data;

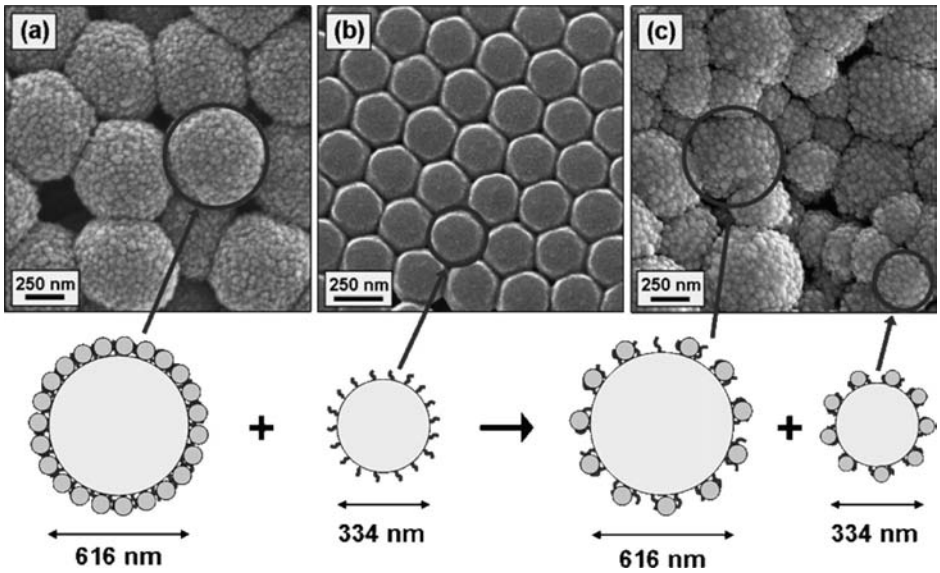

Figure 6. Scanning electron micrographs (and corresponding schematic representation) of (a) P2VP−silica nanocomposite particles prepared by coating a 616 nm sterically stabilized P2VP latex with 20 nm silica (such that the silica surface coverage Θ = 1.00), (b) a 334 nm sterically stabilized P2VP latex, (c) a binary mixture of the P2VP−silica nanocomposite particles shown in image a and the 334 nm P2VP latex (such that the final mean silica surface coverage Θ = 0.50) after silica redistribution has occurred.

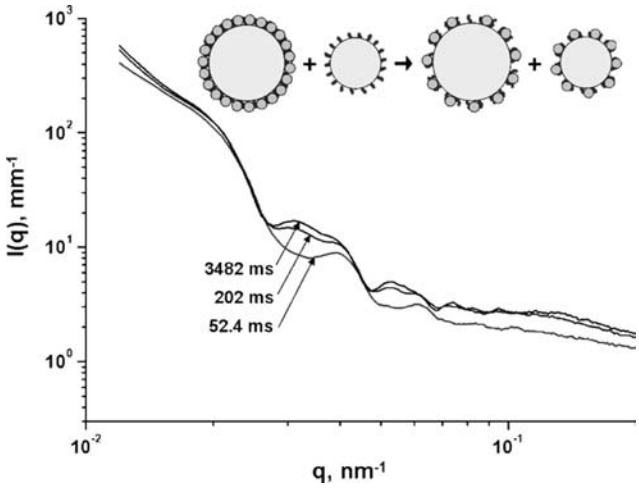

Figure 7. Selected raw SAXS patterns (no background subtraction) obtained during the time-resolved SAXS study of the redistribution of silica between P2VP−silica nanocomposite particles (prepared by the adsorption of a 20 nm silica sol onto a 616 nm PEGMA-stabilized P2VP latex) and a 334 nm P2VP latex.

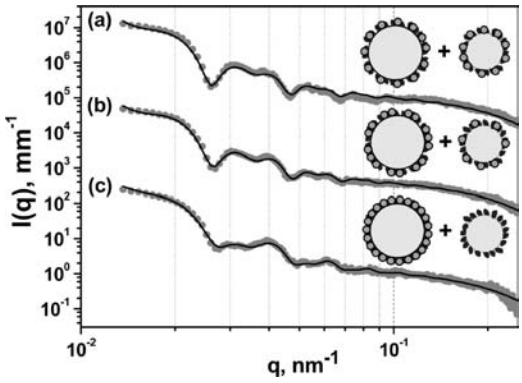

Figure 8. Desmeared SAXS patterns and fits (solid lines) obtained for the redistribution of silica between P2VP−silica nanocomposite particles (prepared by the adsorption of a 20 nm silica sol onto a 616 nm PEGMA-stabilized P2VP latex) and a 334 nm P2VP latex at (a) 3482 ms, (b) 202 ms, and (c) 52.4 ms. Patterns a and b are multiplied by factors of 50 000 and 200, respectively.

water background not subtracted) are presented in Figure 7. The scattering pattern obtained at 3482 ms is equivalent to that observed for a 1.0 w/v % binary mixture of the same P2VP−silica nanocomposite and P2VP latex that had been allowed to equilibrate for a minimum of 1 h at 20 °C. This equilibrium SAXS pattern is qualitatively different from those obtained at 52.4 and 202 ms, which suggests that the particles present in the colloidal dispersion undergo substantial structural evolution over a relatively short time scale.

Much more information about the evolving particle morphologies during silica redistribution can be obtained from the models used to fit the scattering patterns. The particle size parameters obtained from modeling the three individual components alone (i.e., the silica sol and the two P2VP latexes; see Table S2, Supporting Information) were used to fit all the scattering patterns obtained during the time-resolved SAXS experiments for the redistribution of silica. With the exception of the first frame (acquired at 52.4 ms), a good fit to the data was obtained using the three-population model that had been previously applied to the scattering pattern for a mixture of the same P2VP−silica nanocomposite and P2VP latex at equilibrium (see Figure 8a,b). This model comprised one population for the larger core−shell nanocomposite particles, a population for the smaller core−shell nanocomposite particles, and a population for the particulate silica shell that is present in both partially coated nanocomposites.

The resulting structural parameters for the frame acquired at 3482 ms are shown in the third row of Table 1. The calculated volume ratios $[\nu_{silica}/(\nu_{latex\,616nm} + \nu_{latex\,334nm})$ and

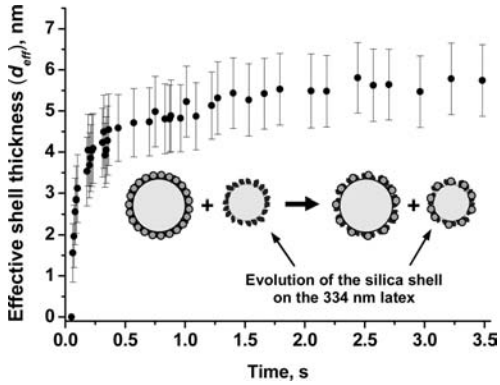

Figure 9. Evolution of the effective silica shell thickness on a 334 nm PEGMA-stabilized P2VP latex after mixing with P2VP−silica nanocomposite particles (prepared by the adsorption of silica onto a 616 nm PEGMA-stabilized P2VP latex).

$\nu_{\text{latex 334nm}}/\nu_{\text{latex 616nm}}$] are comparable to the predicted ratios. The silica shell thicknesses of 5.74 nm for the smaller nanocomposite and 4.50 nm for the larger nanocomposite are very similar to those obtained for the equivalent binary nanocomposite dispersion at equilibrium (5.7 and 4.6 nm, respectively; see Table S2, Supporting Information). Thus, it appears that silica redistribution is complete approximately 3.5 s after mixing the nanocomposite particles and the bare sterically stabilized latex together. A different three-population model was required to obtain a good fit to the scattering pattern acquired at 52.4 ms (Figure 8c). In this case, a core−shell form factor was used for the population of large nanocomposite particles, but only a simple spherical form factor was required to model the population of small latex particles, since this component did not yet possess a shell of adsorbed silica particles.

The three-population model used to fit the scattering patterns obtained during the time-resolved SAXS study of the silica redistribution process incorporates two effective silica shell thicknesses: $d_{\text{eff 616nm}}$ for the shell thickness of the larger nanocomposite and $d_{\text{eff 334nm}}$ for the shell thickness of the resulting smaller nanocomposite that is formed as some of the silica is transferred from the larger nanocomposite particles. As discussed earlier, the shell thickness is correlated to another parameter, ρ_{shell}, which is the scattering length density of the silica shell. In this case, two values of ρ_{shell} are required: $\rho_{\text{shell 616nm}}$ for the density of the silica shell of the larger nanocomposite and $\rho_{\text{shell 334nm}}$ for the density of the silica shell of the smaller nanocomposite. For simplicity, we have chosen to fix both $\rho_{\text{shell 616nm}}$ and $\rho_{\text{shell 334nm}}$ at 12.73×10^{10} cm^{-2}, which represents a *maximum* estimated value for the shell density at full silica monolayer coverage. In doing so, we can allow both $d_{\text{eff 616nm}}$ and $d_{\text{eff 334nm}}$ to fit and thus observe any changes in the magnitudes of these two parameters with respect to time. Figure 9 shows the evolution of the *effective* silica shell thickness for the smaller nanocomposite particles ($d_{\text{eff 334nm}}$) against time. At 52.4 ms, no silica nanoparticles had been transferred from the larger nanocomposite to the small latex, and thus, the silica shell thickness is zero. For all subsequent scattering patterns, there is a rapid initial increase in effective shell thickness, followed by a period of slower growth until equilibrium is reached after around 2.0 s. The maximum effective shell thickness is approximately 5.8 nm. This is lower than the maximum effective shell thickness observed in the case of nanocomposite formation, because the final silica shell is only at submonolayer coverage rather than at full monolayer coverage. Again, we conclude that the time-resolved SAXS experiments are highly reproducible, as the data points from stroboscopic separate experimental runs fall on one general curve of effective shell thickness versus time with relatively little scatter.

It should be emphasized that the fitted parameters obtained from the SAXS models show a much more significant change in $d_{\text{eff 334nm}}$ than in $d_{\text{eff 616nm}}$. This is presumably because there is a substantially greater difference in scattering between the bare 334 nm P2VP latex (at 52.4 ms) and the same latex partially coated in silica (for example, at 202 ms) than there is between the fully silica-coated 616 nm P2VP latex (at 52.4 ms) and the same latex partially coated in silica (for example, at 202 ms). Thus, the three-population model used to analyze the time-resolved SAXS data is much more sensitive to changes in the parameters for the smaller latex, as these particles gain a partial silica shell over time.

Previously, we suggested that a *lower* limit time scale for the kinetics of silica redistribution could be estimated using a zeroth-order approximation based on the Smoluchowski "fast coagulation rate" equation.[18] This approach assumes that silica exchange between nanocomposite and latex particles occurs simply as a result of interparticle collisions caused by Brownian motion. Smoluchowski[38] showed that the half-life, $\tau_{1/2}$, of colloidal particles undergoing rapid coagulation in the absence of any repulsive forces (i.e., assuming only "sticky" interparticle collisions) is given by

$$\tau_{1/2} = 3\eta/(4k_{\text{B}}Tn_{\text{o}})$$

where η is the solution viscosity (8.9×10^{-4} kg s^{-1} m^{-1}), k_{B} is Boltzmann's constant (1.38×10^{-23} J K^{-1}), T is the absolute temperature, and n_{o} is the particle concentration per unit volume. Under our specific experimental conditions ([P2VP−silica]$_{\text{o}}$ = [P2VP latex]$_{\text{o}}$ = 1.0 w/v %, thus $n_{\text{o}} = 2.54 \times 10^{14}$ dm^{-3}), we estimate a $\tau_{1/2}$ of approximately 650 ms for silica exchange at 293 K. If the rate of silica redistribution was equivalent to this Smoluchowski fast coagulation rate, we would expect the shell thickness to have reached 88% of its maximum thickness after three half-lives, i.e. 1950 ms. The data presented in Figure 9 suggest that the silica redistribution process actually reaches equilibrium after approximately 2000 ms. The remarkably good agreement between our experimental data and the calculated half-life demonstrates that, although this diffusion-controlled zeroth-order approximation probably does not fully describe silica redistribution, this phenomenon nevertheless strongly depends on the Brownian collision rate. In a dispersion containing only sterically stabilized latex, interparticle collisions should be fully elastic (non-sticky) due to the steric repulsive potential conferred by the PEGMA polymer chains on the surface of the particles. Similarly, nanocomposite particles are mutually repulsive due to the unfavorable overlap of their respective electric double layers conferred by their anionic silica shells. In contrast, it is not necessarily energetically unfavorable for an electrical double layer to overlap with adsorbed steric stabilizer chains. The absence of any mutual repulsion forces between the nanocomposite particles and the sterically stabilized latex therefore allows these particles to collide freely and hence exchange silica by an entropically driven process. In addition, the rapid rate of silica redistribution confirms that the silica is only weakly adsorbed to the PEG chains on the latex surface, which is in marked contrast to the significantly stronger interaction observed between the polymer and silica components for nanocomposites prepared by in situ polymerization.[13]

The equivalent time-resolved SAXS experiment can be conducted in order to investigate silica redistribution between P2VP−silica nanocomposite particles (prepared by the adsorption of a 20 nm silica sol onto a 334 nm PEGMA-stabilized P2VP latex) and a bare 616 nm P2VP latex (i.e., between small nanocomposite particles and large latex particles). Figure S4 (Supporting Information) shows a plot of the *effective* silica shell thickness for the larger nanocomposite particles ($d_{\mathrm{eff\,616nm}}$) against time. This data set is very similar to that shown in Figure 9 for silica redistribution between large nanocomposite particles and small latex particles. At 52.4 ms, silica nanoparticles have not yet transferred from the smaller nanocomposite to the large latex, and thus the silica shell thickness is zero. For all subsequent scattering patterns, there is a rapid initial increase in effective shell thickness, followed by a period of slower growth until equilibrium is reached at around 1500 ms. The resulting structural parameters for the frame acquired at 3462 ms are shown in the fourth row of Table 1. The calculated volume ratios [$\nu_{\mathrm{silica}}/(\nu_{\mathrm{latex\,616nm}} + \nu_{\mathrm{latex\,334nm}})$ and $\nu_{\mathrm{latex\,334nm}}/\nu_{\mathrm{latex\,616nm}}$] are again comparable with the predicted ratios. There is a discrepancy between the silica shell thicknesses of 7.1 nm (for the smaller nanocomposite) and 4.1 nm (for the larger nanocomposite) obtained for this system and the shell thicknesses of 5.7 nm and 4.5 nm obtained for the addition of small latex particles to large nanocomposite particles (third row in Table 1). This is not unexpected, as in both cases the nanocomposite dispersion (1.0 w/v %) was mixed with the latex dispersion (1.0 w/v %) in a 1:1 ratio by volume. Thus, there is less silica present in the system when the large nanocomposite is mixed with the small latex (final mean silica surface coverage $\Theta = 0.35$) than when the small nanocomposite is mixed with the large latex (final mean silica surface coverage $\Theta = 0.65$).

Finally, it is prudent to highlight why we chose to conduct our time-resolved SAXS studies on silica redistribution using P2VP latexes of differing mean diameters. To illustrate this choice, P2VP−silica nanocomposite particles prepared by the adsorption of a 20 nm silica sol onto a 461 nm PEGMA-stabilized P2VP latex were rapidly mixed with the same bare 461 nm P2VP latex using the stopped-flow equipment at various nanocomposite/latex volumetric ratios. Little or no change in the silica shell thickness was observed over time for experiments attempted at either a 2:1 or 1:1 nanocomposite/latex ratio. Even at a ratio of 1:4, very little difference was observed between the scattering patterns acquired at different times during the silica redistribution process (see Figure S5, Supporting Information). This two-component system (i.e., the bare latex of 461 nm and core−shell particles with a 461 nm core) degenerates into a one-component system during silica redistribution, which limits differentiation between the particles in the fitting process. Nonetheless, good fits to the SAXS data were obtained using the two-population model (previously described for the study of nanocomposite formation by silica adsorption onto latex), where a nanocomposite population with a core−shell form factor was supplemented by a second population for the silica particles. Again, the first frame acquired at 52.4 ms required a different two-population model: the latex population required a spherical form factor. Initially, the concentration of nanocomposite particles was much lower than the four-fold excess concentration of latex particles, thus it was possible to observe an increase in the *effective* silica shell thickness as silica was transferred onto the originally bare latex (see Figure S6, Supporting Information). However, as the amount of silica on the sparsely coated latex particles increased so that all the latex cores in the dispersion had a similar effective shell thickness, the model fitting becomes less stable and the evolution of shell thickness versus time subsequently oscillates chaotically. In addition, the effective silica shell thickness is relatively low due to the large excess of bare latex added to the nanocomposite particles. Thus the final silica shell is very patchy and the core−shell model is actually a physically unrealistic representation of the final nanocomposite morphology for this system.

CONCLUSIONS

Small-angle X-ray scattering is a powerful technique for the particle size analysis of both latexes and nanocomposites. This study demonstrates that SAXS can be used as a nondestructive method for in situ characterization of physicochemical processes in a colloidal system on a millisecond time scale. Scattering patterns obtained for equilibrated 1.0 w/v % colloidal dispersions show that the poly(2-vinylpyridine) (P2VP) latexes are spherical and near-monodisperse. Weight-average particle diameters determined by SAXS analysis are fully consistent with the number-average and intensity-average diameters obtained from electron microscopy and dynamic light scattering. Moreover, SAXS was successfully used to confirm core−shell nanocomposite formation by the physical adsorption of silica nanoparticles onto sterically stabilized P2VP latexes (heteroflocculation route) and also to confirm the spontaneous redistribution of silica that occurs when such nanocomposite particles are challenged by the addition of further sterically stabilized latex.

Time-resolved SAXS can be used to monitor the in situ adsorption of an ultrafine silica sol onto a sterically stabilized latex. Excellent fits to the scattering patterns are obtained using a two-population model, in which a nanocomposite population with a core−shell form factor is supplemented by a population of spherical silica particles. It was not necessary to add a structure factor to account for interparticle interactions within the silica shells, which suggests that this overlayer is relatively disordered. Silica adsorption is very fast: near-monolayer silica coverage is attained within a few seconds. The rate of silica adsorption appears to be strongly dependent on the extent of silica surface coverage, with neither a random sequential adsorption (RSA) model nor a ballistic deposition model adequately describing this process.

Time-resolved SAXS can also be used to monitor the redistribution of silica that occurs when polymer−silica nanocomposite particles are challenged by the addition of sterically stabilized latex. Such scattering experiments work best if there is a mismatch in particle size between the nanocomposite and the latex. Very short time scales are consistent with facile silica exchange occurring simply as a result of interparticle collisions. This interpretation is consistent with a zeroth-order Smoluchowski-type calculation. These findings may have implications for certain commercial formulations of colloidal nanocomposite particles that are based on the addition of ultrafine silica sols to aqueous latexes.[17]

ASSOCIATED CONTENT

Supporting Information. Summary of latex details, schematics of stopped-flow apparatus and core−shell morphologies, additional SAXS patterns, table of SAXS modeling parameters, attempted data fit to ballistic deposition model, evolution of effective silica shell thickness with time for differing and identical

latex diameters, raw scattering patterns for redistribution experiment with identical latexes. This material is available free of charge via the Internet at http://pubs.acs.org.

AUTHOR INFORMATION

Corresponding Author
s.p.armes@sheffield.ac.uk; o.mykhaylyk@sheffield.ac.uk

ACKNOWLEDGMENT

J.A.B. thanks AkzoNobel for an Industrial CASE EPSRC Ph.D. studentship. Dr. P. Greenwood of Eka Chemicals is thanked for donating the aqueous silica sol used in this work. The authors are grateful to ESRF for providing the beamtime and thank the personnel of ID02 station for their helpful assistance with the SAXS experiments. Lee Fielding and Craig Fairgrieve are also thanked for enabling us to maximize the use of our beam time provision. Jan Ilavsky is thanked for support with the Irena SAS package used for SAXS analysis.

REFERENCES

(1) Balmer, J. A.; Schmid, A.; Armes, S. P. *J. Mater. Chem.* **2008,** *18*, 5722–5730.
(2) Zou, H.; Wu, S. S.; Shen, J. *Chem. Rev.* **2008,** *108*, 3893–3957.
(3) Wang, T.; Keddie, J. L. *Adv. Colloid Interface Sci.* **2009,** *147*−*148*, 319–332.
(4) Mitzi, D. B. *Chem. Mater.* **2001,** *13*, 3283–3298.
(5) Burchell, M. J.; Willis, M. J.; Armes, S. P.; Khan, M. A.; Percy, M. J.; Perruchot, C. *Planetary Space Sci.* **2002,** *50*, 1025–1035.
(6) Fujii, S.; Read, E. S.; Binks, B. P.; Armes, S. P. *Adv. Mater.* **2005,** *17*, 1014–1018.
(7) Fujii, S.; Armes, S. P.; Binks, B. P.; Murakami, R. *Langmuir* **2006,** *22*, 6818–6825.
(8) Tiarks, F.; Leuninger, J.; Wagner, O.; Jahns, E.; Wiese, H. *Surf. Coatings Int.* **2007,** *90*, 221–229.
(9) Percy, M. J.; Barthet, C.; Lobb, J. C.; Khan, M. A.; Lascelles, S. F.; Vamvakaki, M.; Armes, S. P. *Langmuir* **2000,** *16*, 6913–6920.
(10) Amalvy, J. I.; Percy, M. J.; Armes, S. P.; Wiese, H. *Langmuir* **2001,** *17*, 4770–4778.
(11) Percy, M. J.; Armes, S. P. *Langmuir* **2002,** *18*, 4562–4565.
(12) Schmid, A.; Scherl, P.; Armes, S. P.; Leite, C. A. P.; Galembeck, F. *Macromolecules* **2009,** *42*, 3721–3728.
(13) Dupin, D.; Schmid, A.; Balmer, J. A.; Armes, S. P. *Langmuir* **2007,** *23*, 11812–11818.
(14) Schmid, A.; Tonnar, J.; Armes, S. P. *Adv. Mater.* **2008,** *20*, 3331–3336.
(15) Schmid, A.; Armes, S. P.; Leite, C. A. P.; Galembeck, F. *Langmuir* **2009,** *25*, 2486–2494.
(16) Balmer, J. A.; Armes, S. P.; Fowler, P. W.; Tarnai, T.; Gaspar, Z.; Murray, K. A.; Williams, N. S. J. *Langmuir* **2009,** *25*, 5339–5347.
(17) Greenwood, P.; Lagnemo, H. U.S. Patent No. 7,544,726, 2009.
(18) Balmer, J. A.; Mykhaylyk, O. O.; Fairclough, J. P. A.; Ryan, A. J.; Armes, S. P.; Murray, M. W.; Murray, K. A.; Williams, N. S. J. *J. Am. Chem. Soc.* **2010,** *132*, 2166–2168.
(19) Balmer, J. A.; Le Cunff, E. C.; Armes, S. P.; Murray, M. W.; Murray, K. A.; Williams, N. S. J. *Langmuir* **2010,** *26*, 13662–13671.
(20) Dupin, D.; Rosselgong, J.; Armes, S. P.; Routh, A. F. *Langmuir* **2007,** *23*, 4035–4041.
(21) Zhang, J. Y.; Li, Y. T.; Armes, S. P.; Liu, S. Y. *J. Phys. Chem. B* **2007,** *111*, 12111–12118.
(22) Panine, P.; Finet, S.; Weiss, T. M.; Narayanan, T. *Adv. Colloid Interface Sci.* **2006,** *127*, 9–18.
(23) Grillo, I. *Curr. Opin. Colloid Interface Sci.* **2009,** *14*, 402–408.
(24) Pontoni, D.; Narayanan, T.; Rennie, A. R. *Langmuir* **2002,** *18*, 56–59.
(25) Bolze, J.; Peng, B.; Dingenouts, N.; Panine, P.; Narayanan, T.; Ballauff, M. *Langmuir* **2002,** *18*, 8364–8369.
(26) Polte, J.; Erler, R.; Thunemann, A. F.; Sokolov, S.; Ahner, T. T.; Rademann, K.; Emmerling, F.; Kraehnert, R. *ACS Nano* **2010,** *4*, 1076–1082.
(27) Schmolzer, S.; Grabner, D.; Gradzielski, M.; Narayanan, T. *Phys. Rev. Lett.* **2002,** *88*, 258301.
(28) Sztucki, M.; Narayanan, T. *J. Appl. Crystallogr.* **2007,** *40*, S459–S462.
(29) Lake, J. A. *Acta Crystallogr.* **1967,** *23*, 191–194.
(30) Ilavsky, J.; Jemian, P. R. *J. Appl. Crystallogr.* **2009,** *42*, 347–353.
(31) Zhang, F.; Long, G. G.; Jemian, P. R.; Ilavsky, J.; Milam, V. T.; Lewis, J. A. *Langmuir* **2008,** *24*, 6504–6508.
(32) Muratov, A.; Moussaid, A.; Narayanan, T.; Kats, E. I. *J. Chem. Phys.* **2009,** *131*, 054902.
(33) Evans, J. W. *Rev. Mod. Phys.* **1993,** *65*, 1281–1329.
(34) Adamczyk, Z.; Warszynski, P. *Adv. Colloid Interface Sci.* **1996,** *63*, 41–149.
(35) Cross, W. M.; Ma, S.; Winter, R. M.; Kellar, J. J. *Colloids Surf., A* **1999,** *154*, 115–125.
(36) Jullien, R.; Meakin, P. *J. Phys. A: Math. Gen.* **1992,** *25*, L189–L194.
(37) Thompson, A. P.; Glandt, E. D. *Phys. Rev. A* **1992,** *46*, 4639–4644.
(38) Smoluchowski, M. *Phys. Z.* **1916,** *17*, 557; **1916,** *17*, 585.